International Journal of New Technology and Research (IJNTR)
ISSN:2454-4116, Volume-2, Issue-7, July 2016 Pages 07-15

A Simplified and Universal Mechanism Model for Prediction of Gallium Nitride Thin Film Growth Through Numerical Analysis

C.K. Hu, C.J. Chen,T.C. Wei, Tomi T. Li, C. C. Wang, C. Y. Huang, Y.J. Lin

***Abstract*—The crucial parameter required for predicting epitaxial thin film growth rates and uniformity is the chemical mechanism occurring in the gas phase and at the surface. To date, few studies have investigated the gallium nitride epitaxial mechanism in solid state lighting. A simplified chemistry derived from experimental observation has been used for this purpose. In this study, three numerical mechanism models are presented for verifying the growth rate of the gallium nitride (GaN) mechanism, and their results are compared with the growth rate results of previous literature studies. To reduce the calculation time of numerical analysis in commercial software, a numerical procedure is performed for simplifying the complicated mechanism of an epitaxial thin-film process. The mechanism models are developed through rate of production analysis. All the solution results could be compared in one schematic diagram, and the differences among these three mechanisms are extremely pronounced in high temperatures. The simplified reaction mechanisms are then used as input for a two-dimensional computational fluid dynamics code FLUENT, enabling the accurate prediction of growth rates. Validation studies are presented for two different laboratory-scale reactors. For each study, the predictions reasonably agree with the experimental data, indicating the universality of the reaction mechanisms.**

***Index Terms*—MOCVD, LED, mechanism, GaN, numerical, thin film.**

I. INTRODUCTION

Metal organic chemical vapor deposition (MOCVD) is a crucial process [1~4] for manufacturing compound semiconductor devices. Through the force convection mechanism, thin films are deposited on solid substrates from the gas inlet to the gas outlet. During this process, the reactant vapors enter the chamber from the top of the showerhead and flow down vertically into the reactor.

Chih-Kai, Hu, Department of Mechanical Engineering, National Central University, Taoyuan 3320, Taiwan (R.O.C.).
Chun-Jung, Chen, Department of Chemical Engineering, Chung Yuan Christian University, Taoyuan 320, Taiwan (R.O.C.).
Ta-Chin Wei, Professor, Department of Chemical Engineering, Chung Yuan Christian University, Taoyuan 320, Taiwan (R.O.C.).
Ting-Tung,Li (Tomi T. Li), Professor, Department of Mechanical Engineering, National Central University, Taoyuan 3320, Taiwan (R.O.C.).
Ching-Chiun, Wang, Industrial Technology Research Institute, Hsinchu 300, Taiwan (R.O.C).
Chih-Yung, Huang, Industrial Technology Research Institute,Hsinchu 300, Taiwan (R.O.C).
Yi-Jiun Lin, Industrial Technology Research Institute, Hsinchu 300, Taiwan (R.O.C).

Upon contacting the surface of the susceptor, the reactant vapors flow, radially outward above the susceptor and wafer then finally exhaust through the outlet. By using this unique technique, a high-quality GaN epitaxial thin film was obtained for the first time on a sapphire wafer [5~7].

Design on simulation, which is based on commercial numerical software, is now widely used in the semiconductor industry in the optimization and troubleshooting of epitaxial growth processes that occur on the substrate [8~9]. Furthermore, it is commonly employed in reactor design. In the past 20 years, only a few studies have investigated the GaN mechanism; therefore, the experimental data available for III-nitride MOCVD growth chemistry are extremely limited, particularly the chemical kinetic rate data in the Arrhenius equation. Although a simplified reaction model is introduced by S. A. Safvi [10], several features of the GaN growth chemistry can be identified that have been established by experimental and numerical computational studies [10~14], but the GaN thin film mechanism is still unclear for many years.

A complicated chemistry method derived from theab initio quantum chemistry methods developed in 2005 is used for growth rate prediction [15]. Such detailed reaction mechanisms, comprising mostly elementary and ring reactions, have the advantage of requiring little or no calibration by using experimental data. However, for a complicated mechanism, a single computer has difficulty in rapidly obtaining a solution, and the calculation time is considerably extensive.

For the two-dimensional (2D) calculation, CFD modeling has recently become one of the critical tools used for designing and optimizing the performance of an MOCVD reactor [16~19]. For a complicate mechanism, although the accuracy is sufficient, the computational capacity is extremely high, the calculation time is always up to few days and difficult to calculate using a standard computer.By using the parallel computing may be the best way to solve this problem, but the fund cost is too high to achieve. This study used the complicated chemical mechanism from previous studies [15], which is simplified through the rate of production (ROP) analysis (CHEMKIN, 0-dimensional calculation), and the goal is to develop a simplified mechanism can easy calculated by a standard computer to predict the GaN growth in blue-LED process.And it can be used as the key equipment design for in general academia and industry.

II. THE NUMERICAL MODELING DETAILS

Procedure for the numericalmodeling

Fig. 1 illustrates the complete procedure for this numerical modeling. The first step is 0-D computation, including an ROP optimized analysis for the mechanism model (Complete model, Reduced model, and New model) and general theory. In the next step, we import the most simplified model (New model) for the 2D software, FLUENT, to calculate the growth rate in two examples. Fig. 2 is the brief procedure for development of growth rate; this figure describes how we obtain the growth rate for GaN thin film.

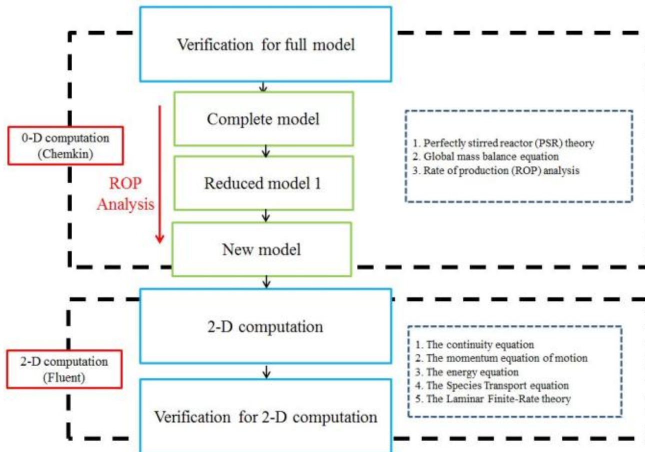

Fig. 1. Schematic procedure of the Complete numericalmodeling.

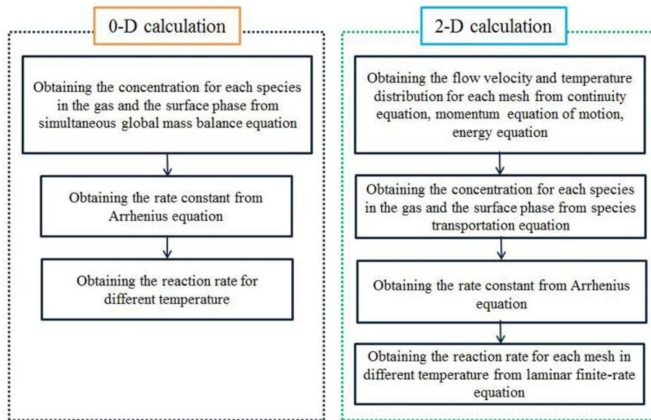

Fig. 2. Schematic procedure for the 0 and 2-D numerical analysis

A. Governing equation in the 0-dimensional analysis

In CHEMKIN, the Perfectly Stirred Reactor (PSR) model is used in this study. The contents of a PSR are assumed to be nearly spatially uniform due to high diffusion rates of forced mixing. In other words, the rate of conversion of reactants to products is controlled by chemical reaction rates and not by mixing processes. Thus we consider that the reactor is limited by reaction kinetics. Mass transport to the reactor walls is assumed to be infinitely fast. Therefore, the relative importance of surface reactions to gas-phase reactions is determined only by the surface to volume ratios of each material and the relative reaction rates. In this section, we introduce the equation that be used in this study.

Global mass balance equation

$$\frac{dm}{dt} = \dot{m}_{in} - \dot{m}_{out} + \dot{m}_{reaction} \quad (1)$$

m is the mass in the reactor, $\dot{m}_{in,out}$ is the mass flows in and out to the system. $\dot{m}_{reaction}$ is the reaction term includes generation and consumption work in both gas and surface phase.

Rate of production (ROP) analysis

In CHEMKIN, ROP analysis can help user determine the most dominant reaction paths in some complicated reaction mechanisms, the general expression for this analysis is

$$ROP_{i,\,production} = \frac{R_{i.\,production}}{\sum_j R_{j,production}} \quad (2)$$

$$ROP_{i,\,consumption} = \frac{R_{i,\,consumption}}{\sum_j R_{j,consumption}} \quad (3)$$

ROP analysis enables the rapid identification of dominant reaction paths. It indicates each path by percentage on the x-axis (production or consumption), for example, 0.1=10%, 0.2=20%, respectively. The y-axis shows the reaction detail for different temperature.$R_{i.\,production}$ is production rate for the species i, $\sum_j R_{j,production}$ is the total production rate for species i, $R_{i,\,consumption}$ is consumption rate for the species i, $\sum_j R_{j,consumption}$ is the total consumption rate for the species i.

B. Governing equation in the 2-dimensional (2D) analysis

The following 5 equations listed systematically are for 2-dimentional computation in FLUENT including the final calculation of obtained growth rate of GaN

Continuity equation

The general integral mass conservation equation in differential form is given by

$$\nabla \cdot \vec{v} = 0 \quad (4)$$

ρ is the density of the fluid, $\vec{v}$ is the velocity vector, and t stands for times.

Momentum equation of motion

The general Navier–Stokes equation is

$$\rho \frac{\partial \vec{v}}{\partial t} + \rho(\vec{v} \cdot \nabla \vec{v}) = -\nabla p + \mu \nabla \vec{v} + \rho \vec{f} \quad (5)$$

For an incompressible fluid, the left side is momentum difference of the system,μ is the viscosity coefficient and$\vec{f}$ is the body force.

Energy equation

$$\rho \frac{\partial e}{\partial t} + \rho(\vec{v} \cdot \nabla e) = -p(\nabla \cdot \vec{v}) + \nabla \cdot (k \nabla T) \quad (6)$$

This equation involves the total work done by pressure, work done by viscous force, k is the thermal conductivity for fluid, T is temperature, $e$is the energy per unit mass for fluid.

Species transportation equation

This conservation equation is expressed in the following form:

$$\frac{\partial}{\partial t}(\rho Y) + \nabla \cdot (\rho \vec{v} Y) = -\nabla \cdot \dot{J} + R + S \qquad (7)$$

Where$R$is the net rate of production of species by chemical reaction, Y is the local mass fraction of each species and S is the rate of creation by addition from the dispersed phase plusany user-defined sources.

Laminar finite-rate equation and Arrhenius equation

Laminar finite-rate equation is written in general form as follows:

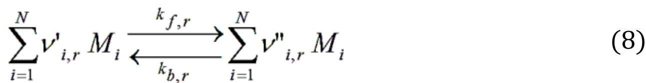

$$\sum_{i=1}^{N} V'_{i,r} M_i \underset{k_{b,r}}{\overset{k_{f,r}}{\rightleftarrows}} \sum_{i=1}^{N} V"_{i,r} M_i \qquad (8)$$

N is number of chemical species in the system, $V'_{i,r}$ is the stoichiometric coefficient for reactant i in reaction r, $V"_{i,r}$is the stoichiometric coefficient for product i in reaction r, symbol denoting species i, $M_i$is symbol denoting species i, $k_{f,r}$ is the forward rate constant for reaction r, $k_{b,r}$ = backward rate constant for reaction r.

The forward rate constant (growth rate) is computed using the Arrhenius expression

$$k_{f,r} = AT^n e^{-Ea/RT} \qquad (9)$$

Where $A$is the pre-exponential factor, B is the temperature exponent, Ea is the activation energy for the reaction, and R is the universal gas constant.

2D numerical assumption

In this study, the following assumptions are made for the 2D model: (1) the gas mixture is treated as a continuum; (2) steady state is considered; (3) axisymmetric behavioris assumed; (4) radiation between the walls is neglected; and (5) incompressible ideal gas behavior is assumed.

Boundary condition

The simulations described in this section were performed through the commercial fluid dynamics code FLUENT, which employs the finite volume method to solve governing fluid equations of mass, momentum, energy, and species conservation laws in a stationary state; The gas-flow conditions in various MOCVD reactors and their chemical conditions can be calculated using FLUENT. Table 7 lists the used in the numerical simulation parameters. The boundary conditions for the model are as follows. No slip condition are imposed on the reactor wall anda velocity boundary condition is specified as the showerhead or nozzle gas inlet, which is obtained from the given volume flow rate. The temperature and species mole fraction are also specified for the inlet. For the outlet, the outflow boundary condition is selected, which presumes the fully developed flow at the outlet. For the wall, zero velocity, constant temperature, zero species gradient, and zero thermal flux are assumed. The susceptor temperature is maintained at 1323K, whereas the temperatures of all the other side walls are set to 27 °C because of water cooling; the operating pressure is set in the range 100~200torr.

III. Results and Discussion

A. Computation of the Complete mechanism model

A mathematical representation is developed for the Complete mechanism model involving ROP analysis through the 0D dimension software CHEMKIN. Tables 1 and 2 summarize the gas and surface reaction mechanisms [15]. The Arrhenius coefficients and activation energy are all temperature sensitive;the small pressure difference will not affect the final conclusion and computation. So, the pressure difference between derivative and process is ignoring.

The gas reaction mechanism considers several aspects including the pyrolysis reactions for tri-methyl gallium (TMG), di-methyl gallium (DMG), and monomethyl gallium (MMG), and the adduct reactions with NH_3 and CH_3; interaction among CH_3, H_2, and H; and finally, the pyrolysis reaction for adducts. TMG and MMG decompose slowly because of their large activation energy barriers; however, the pyrolysis reaction of DMG to MMG is rapid. Therefore, the conversion of TMG to MMG is rapid at high temperatures, and the concentration of MMG is expected to be high at higher temperatures. Therefore, MMG and MMG:NH_3 are expected to be the dominant gallium-containing precursors at high temperatures, whereas TMG and TMG:NH_3 are expected to contribute to the deposition at low temperatures. For the surface reaction, Table 2 lists three paths and Table 3 is the compositions for chemical compounds on the surface.

Path 1 displays the ring reaction between MMG and NH_3. First, the MMG in the gas phase is absorbed by the substrate to form the surface site MMG(S) which then interacts with NH_3 in the gas region and forms COMPM1(S). This procedure is repeated until COMPM5(S) is formed. COMPM5(S) is desorbed by a CH_3 radical to form a ring structure RINGM1, which is then attached to a nearby surface Ga(S). Finally, the hydrogen atoms H_2 are eliminated, resulting in GaN formation.

Path 2 for GaN formation starts from the adsorption at the surface site $GaNH_2$(S). This species can directly be formed from the gas phase reaction of the MMG and NH_3 or through the reaction of the adsorbed Ga(S) and adsorbed NH_2(S). $GaNH_2$(S) then absorbs the MMG and NH_3 in the gas phase to form the compound COMPMM1(S). Similar to Path 1, this process is repeated until the elimination of CH_4 to produce a ring structure RINGM1(S). Finally, the ring absorbs CH_3 radicals from each Ga atom of the ring followed by the elimination of CH_4, resulting in GaN formation.

In Path 3, TMG adsorbs on N(S) to form TMG(s). NH_3 is then adsorbed by TMG(S) to form TCOM1(S). Moreover, TCOM1 can be formed by the adduct TMG:NH_3 in the gas phase, which is directly absorbed by the surface N(S). Similar to the processes in Paths 1 and 2, this procedure repeats until

a complex TCOM3(S) is formed. Finally, this complex TCOM3(S) eliminates two molecules of CH_4 to produce GaN. To verify the accuracy of our CHEMKIN software, we incorporated the Complete mechanism model presented in Tables 1 and 2 into the solver. Table 4 lists the input parameters for the calculation of the growth rate. Fig. 3 illustrates the predicted result compared with the results of previous studies.

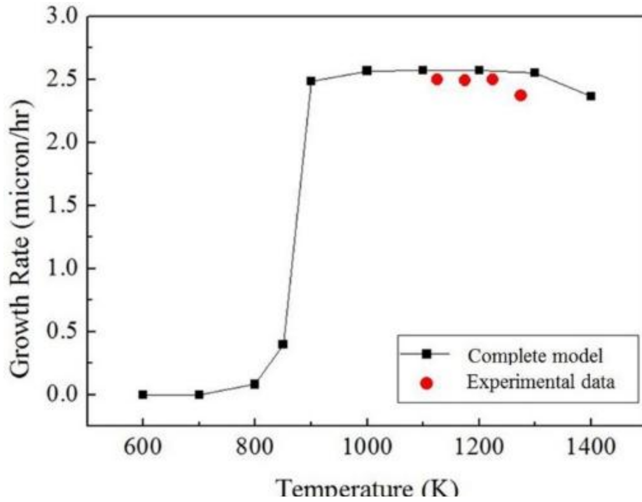

Fig. 3. Result of the Complete mechanism model vs. literaturedata [11].

On the basis of the aforementioned mechanisms, we observe that in a high-temperature zone, this numerical result is precisely matched to the experimental data. This section displays that the numerical code CHEMKIN is a reliable software tool, and we used it to describe chemical mechanisms in this study. We describe the simplified procedure in the next section.

Table 1
Gas-phase mechanism for the Complete model [15]. The unit of Ea is kJ/mol.

	$k=AT^n e^{-Ea/RT}$							A	n	Ea
G1	TMG	=	DMG	+	CH_3			1.00E+47	-9.18	76996
G2	DMG	=	MMG	+	CH_3			7.67E+43	-9.8	34017
G3	MMG	=	Ga	+	CH_3			1.68E+30	-5.07	84030
G4	TMG	+	NH_3	→	$TMG:NH_3$			2.28E+34	-8.31	3115
G5	TMG	+	NH_3	→	$DMG:NH_2$	+	CH_4	1.70E+04	2	19969
G6	DMG	+	NH_3	→	$DMG:NH_3$			4.08E+31	-7.03	3234
G7	DMG	+	NH_3	→	$MMG:NH_2$	+	CH_4	5.30E+05	1.56	20744
G8	MMG	+	NH_3	→	$MMG:NH_3$			7.95E+24	-5.21	2094
G9	MMG	+	NH_3	→	$GaNH_2$	+	CH_4	8.10E+05	1.3	17722
G10	NH_3	+	CH_3	→	NH_2	+	CH_4	3.31E+03	2.51	9859
G11	CH_3	+	H_2	→	CH_4	+	H	1.20E+12	0	12518
G12	TMG	+	H	→	DMG	+	CH_4	5.00E+13	0	10036
G13	DMG	+	H	→	MMG	+	CH_4	5.00E+13	0	10036
G14	$TMGNH_3$	→	MMG	+	$2CH_3$	+	NH_3	1.33E+44	-8.24	77791
G15	CH_3	+	H	+	M	→	CH_4 + NH_3	2.40E+22	-1	0
G16	$2CH_3$	=	C_2H_6					2.00E+13	0	0
G17	2H	+	M	=	H_2	+	M	2.00E+16	0	0

Table 2
Surface-phase mechanism of the Complete model [15]. The unit of Ea is kJ/mol.

	Path 1, $k=AT^n e^{-Ea/RT}$								A	n	Ea
1	MMG	+	N(S)	→	MMG(S)				1.16E+05	2.98	0
2	MMG(S)	→	MMG	+	N(S)				1.12E+14	0.55	107673
3	NH_3	+	MMG(S)	→	COMPM1(S)				3.35E+07	3.33	0
4	COMPM1(S)	→	NH_3	+	MMG(S)				5.70E+13	-0.16	8146
5	MMG	+	COMPM1(S)	→	CH4	+	COMPM2(S)		1.23E+10	3.22	23446
6	NH_3	+	COMPM2(S)	→	COMPM3(S)				3.35E+07	3.33	0
7	COMPM3(S)	→	NH_3	+	COMPM2(S)				5.70E+13	-0.161	8146
8	MMG	+	COMPM3(S)	→	CH_4	+	COMPM4(S)		1.23E+10	3.22	23446
9	NH_3	+	COMPM4(S)	→	COMPM5(S)				3.35E+07	3.33	0
10	COMPM5(S)	→	NH_3	+	COMPM4(S)				5.70E+13	-0.161	8146
11	COMPM5(S)	→	CH4	+	RINGM1(S)				1.23E+07	3.22	23446
12	Ga(S)	+	RINGM1(S)	→	RINGM2(S)	+	N(S)		3.35E+07	3.33	0
13	RINGM2(S)	→	$3H_2$	+	3GaN(B)	+	Ga(S)		3.68E+09	2.05	59610
	Path 2, $k=AT^n e^{-Ea/RT}$								A	n	Ea
14	CH3	+	Ga(S)	→	MMG(S)				1.76E+09	1.39	0
15	MMG(S)	→	CH3	+	Ga(S)				4.54E+13	0.0346	79480
16	NH2	+	Ga(S)	→	NH2(S)				3.17E+08	1.83	0
17	GaNH2	+	N(S)	→	GaNH2(s)				2.27E+06	2.247	0
18	GaNH2(S)	→	GaNH2	+	N(S)				4.83E+13	0.614	83881
19	COMPMM1(S)	→	CH4	+	GaNH2(S)				1.49E+11	0.609	25950
20	MMG	+	GaNH2(S)	→	COMPMM1(S)				1.16E+05	2.98	0
21	NH3	+	COMPMM1(S)	→	COMPMM2(S)				3.35E+07	3.33	0
22	COMPMM2(S)	→	CH4	+	COMPMM3(S)				1.49E+11	0.609	25950
23	MMG	+	COMPMM3(S)	→	COMPMM4(S)				1.16E+05	2.98	0
24	NH3	+	COMPMM4(S)	→	COMPMM5(S)				3.35E+07	3.33	0
25	COMPMM5(S)	→	CH_4	+	RINGM1(S)				1.49E+11	0.609	25950
26	NH_2(S)	→	NH_2	+	Ga(S)				1.45E+14	0.09	59786
27	COMPMM1(S)	→	MMG	+	$GaNH_2$(S)				1.00E+14	0.55	42819
28	COMPMM2(S)	→	NH_3	+	COMPMM1(S)				5.70E+13	-0.1	8146
29	COMPMM4(S)	→	MMG	+	COMPMM3(S)				1.00E+14	0.55	42819
30	COMPMM5(S)	→	NH_3	+	COMPMM4(S)				5.70E+13	-0.1	8146
31	Ga	+	N(S)	→	Ga(S)				1.00E+11	1.5	0
32	Ga(S)	+	NH_2(S)	→	$GaNH_2$	+	Ga(S)		1.00E+25	0	0
33	Ga(S)	→	Ga	+	N(S)				1.00E+13	0	45168
34	$6CH_3$	+	RINGM2(S)	→	COM1(S)				7.55E+07	2.31	0
35	COM1(S)	→	$6CH_3$	+	RINGM2(S)				1.00E+13	0.71	45506
36	COM1(S)	→	$6CH_4$	+	3GaN(B)	+	Ga(S)		4.00E+12	0	49675
	Path 3, $k=AT^n e^{-Ea/RT}$								A	n	Ea
37	TMG	+	N(S)	→	TMG(S)				1.16E+05	2.98	0
38	NH_3	+	TMG(S)	→	TCOM1(S)				3.35E+07	3.33	0
39	TCOM1(S)	→	CH_4	+	TCOM2(S)				1.49E+11	0.609	32785
40	Ga(S)	+	TCOM2(S)	→	TCOM3(S)	+	N(S)		3.35E+07	3.33	0
41	TCOM3(S)	→	$2CH_4$	+	GaN(B)	+	Ga(S)		1.49E+11	0.609	49675
42	TMG(S)	→	TMG	+	N(S)				1.12E+14	0.55	49675
43	TCOM1(S)	→	NH_3	+	TMG(S)				5.70E+13	-0.161	11922
44	$TMG:NH_3$	+	N(S)	→	TCOM1(S)				1.16E+05	2.98	0
45	TCOM1(S)	→	$TMG:NH_3$	+	N(S)				1.12E+14	0.55	49675
46	TCOM1(S)	→	$2CH_3$	+	MMG(S)	+	NH_3 +N(S)		1.12E+14	0.55	107673
47	$MMGNH_3$	+	N(S)	→	COMPM1(S)				1.16E+05	2.98	0
48	COMPM1(S)	→	$MMG:NH_3$	+	N(S)				1.12E+14	0.55	107673
49	$MMG:NH_3$	+	COMPM1(S)	→	CH_4	+	COMPM3(S)		1.23E+10	3.22	23446
50	$MMG:NH_3$	+	COMPM3(S)	→	CH_4	+	COMPM5(S)		1.23E+10	3.22	23446
51	$MMG:NH_3$	+	$GaNH_2$(S)	→	COMPMM2(S)				1.16E+05	2.98	0
52	$MMG:NH_3$	+	COMPMM3(S)	→	COMPMM5(S)				1.16E+05	2.98	0

Table 3
The chemical compositions for the chemical compounds on the surface [15]

Compounds names	Chemical formula
COMPM1(S)	NH3·MMG(S)
COMPM2(S)	Ga·NH2·MMG(S)
COMPM3(S)	NH3·Ga·NH2·MMG(S)
COMPM4(S)	Ga·NH2·Ga·NH2·MMG(S)
COMPM5(S)	NH3·Ga·NH2·Ga·NH2·MMG(S)
RINGM1(S)	NH2·Ga·NH2·Ga·NH2·Ga(S)
RINGM2(S)	(S)NH2·Ga·NH2·Ga·NH2·Ga(S)
COMPMM1(S)	MMG·GaNH2(S)
COMPMM2(S)	NH3·MMG·GaNH2·Ga(S)
COMPMM3(S)	NH2·Ga·NH2·Ga(S)
COMPMM4(S)	MMG·NH2·Ga·NH2·Ga(S)
COMPMM5(S)	NH3·MMG·NH2·Ga·NH2·Ga(S)
TCOM1(S)	NH3·TMG(S)
TCOM2(S)	NH2·DMG(S)
TCOM3(3)	(S)NH2·DMG(S)
COM1(S)	RINGM2(S)·CH3 complex

Table 4
Process parameters for the 0-D model [11].

Volume flow rate	values
Standard liter per minute	
TMGa flow rate (μmol/min)	7.48×10^{-4}
NH_3 flow rate (Slm)	6
H_2 flow rate (Slm)	7.1
Parameter	**value**
Initial pressure (torr)	140
Susceptor temperature (K)	600 ~ 1400
Reactor initial temperature (K)	300
Gas inlet temperature (K)	300
V/III ration	2000

B. Development of the Completemechanism model

For the LED industry, rapidly and accurately predicting epitaxial uniformity and growth rate is critical. The accuracy is verified using the aforementioned 0D calculation. For the Complete model, the reaction number of the Complete mechanism is up to 69,as listed in Tables 1 and 2. Therefore, we must simplify the Complete model. ROP analysis is used for determining the contribution of each reaction to the net production or destruction rate of a species. It is particularly useful for 0D systems, where the computational expense for

the added calculations is low, and the data can be considered from a large reactor set. Therefore, ROP analysis rapidly identifies dominant reaction paths. Fig. 4 displays the ROP analysis of a Complete model and the reaction path at different temperatures for producing a GaN thin film.For a blue-LED process, the critical process temperature are 1300~1400 K.

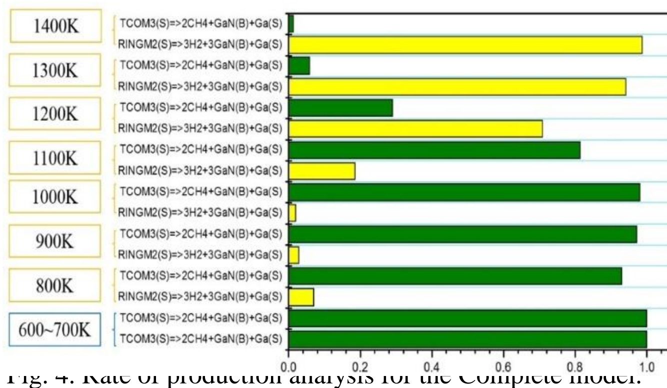

Fig. 4. Rate of production analysis for the Complete model.

For a process temperature greater than 1300 K, the most dominant reaction paths are reaction number 13 and 41 in table 1, respectively. The percentage of the pyrolysis reaction for RINGM2(S) is extremely significant and can be up to 90%. Fig. 5 depicts the schematics for Paths 1 and 2. Path 1 displays the successive reaction between MMG and NH_3.

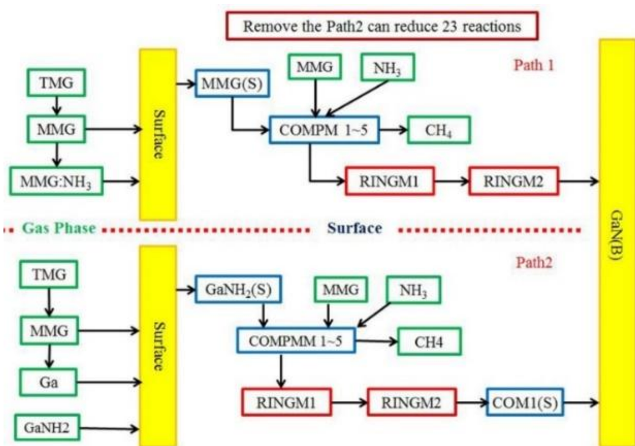

Fig. 5. Schematic for Paths 1 and 2.

The MMG in the gas phase is absorbed by the substrate to form the surface site MMG(S) and then interacts with NH_3 until the ring structure RINGM2 is formed. The hydrogen atoms H_2 are then eliminated, resulting in GaN formation. Similar to that in Path 1, the process in Path 2 repeats until eliminating CH_4; a ring structure RINGM2(S) is then produced; however, the source for Path 2 is $GaNH_2$. The ROP analysis in Fig. 4 demonstrates that at high temperatures (1300–1400 K), the reaction for $GaNH_2$ in Path 2 almost does not occur.

Figs. 6, 7, and 8 depict the ROP analyses for species consumption of TMG, DMG, and MMG, respectively.

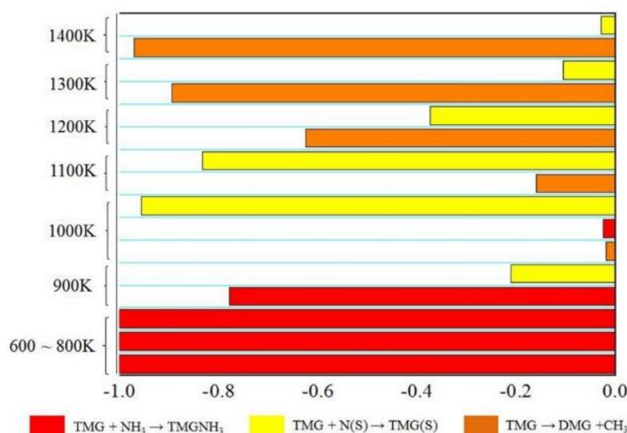

Fig. 6. ROP analysis for TMGa in the gas phase.

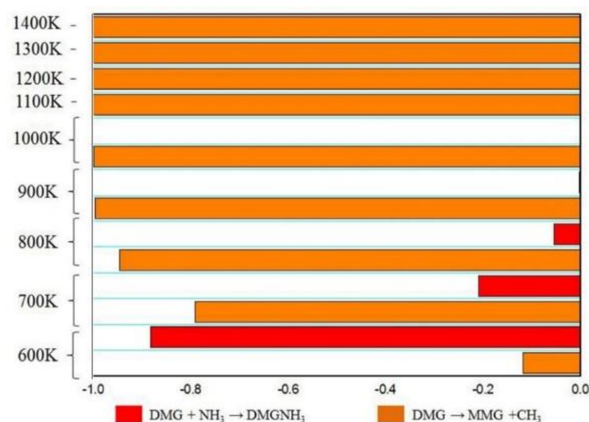

Fig. 7. ROP analysis for DMGa in the gas phase.

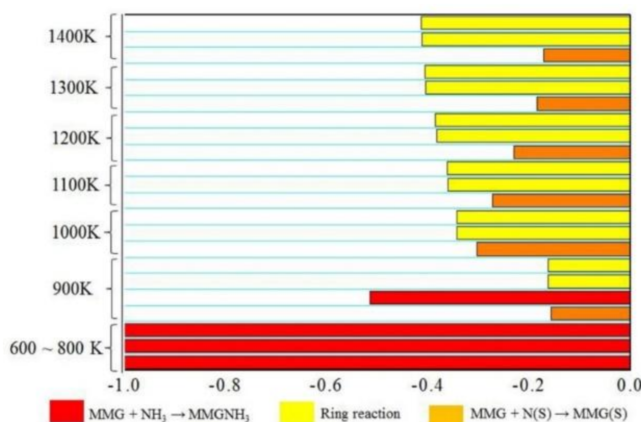

Fig. 8. ROP analysis for MMGa in the gas phase.

Figs. 6 and 7 display three consumption paths for TMGand DMG in the gas phase; however, at high temperatures, TMG tends to convert to DMG. A low percentage of TMG converts to TMG(S), and DMG tends to decompose into MMG in high-temperature zones. Moreover, as displayed in Fig. 8, MMG is consumed in the ring reaction or converts to MMG(S) at the surface. To sum up, we can conclude that nearly no CH_3 exists in the gas phase for Path 2. Thus, Path 2 is not crucial in high-temperature zones. From [15], the Upper way reaction (ring structure) is the main way to produce the GaN, every pathway is first connected by three Ga sources and three N sources, then it connected by another active point, finally release the CH_4 to produce the GaN, but

this is too complicate to calculate. So, in this section, this study assumed thata single direction wayto produce GaN, when the Ga source adsorbed by the surface, the NH_3 in thegas phase will physically adsorbed on the surface, when the energy is sufficient, it will release CH_4, $H_2$to form GaN.

Hence, we delete Path 2 and the ring structure for Path 1 for simplifying the Complete model. Fig. 9 displays a schematic of the new Path 1 (reduced surface mechanisms).

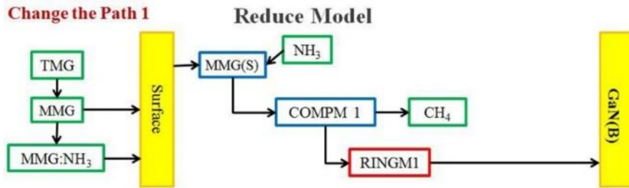

Fig. 9. Schematic diagram for the new Path 1.

Table 5 lists the new form of surface mechanisms in Reduced model (gas mechanism remains the same from complicate mechanism) for Path 1.

Table 5
Surface mechanisms (Path 1+Path 3) are considered for the Reduced model.

	Reaction	A	n	Ea
1	MMG + N(S) → MMG(S)	1.16E+05	2.98	0
2	MMG(S) → MMG + N(S)	1.12E+14	0.55	107673
3	NH_3 + MMG(S) → COMPM1(S)	3.35E+07	3.33	0
4	COMPM1(S) → NH_3 + MMG(S)	5.70E+13	-0.16	8146
5	COMPM1(S) → CH_4 + COMPM2(S)	1.23E+10	3.22	23446
6	COMPM2(S) → H_2 + GaN(B) + N(S)	3.68E+09	2.05	59610
7	TMG + N(S) → TMG(S)	1.16E+05	2.98	0
8	TMG(S) → TMG + N(S)	1.12E+14	0.55	49675
9	NH_3 + TMG(S) → TCOM1(S)	3.35E+07	3.33	0
10	TCOM1(S) → NH_3 + TMG(S)	5.70E+13	-0.161	11922
11	TCOM1(S) → CH_4 + TCOM2(S)	1.49E+11	0.609	32785
12	TCOM2(S) → $2CH_4$ + GaN(B) + N(S)	1.49E+11	0.609	49675
13	$TMGNH_3$ + N(S) → TCOM1(S)	1.16E+05	2.98	0
14	TCOM1(S) → $TMGNH_3$ + N(S)	1.12E+14	0.55	49675
15	TCOM1(S) → $2CH_3$ + MMG + NH_3 + N(S)	1.12E+14	0.55	107673
16	$MMGNH_3$ + N(S) → COMPM1(S)	1.16E+05	2.98	0
17	COMPM1(S) → $MMGNH_3$ + N(S)	1.12E+14	0.55	107673

Fig. 10 provides the final predicted result (include path 1 and path 3) of this new form of mechanism for the Reduced model; the result strongly agrees with that of the Complete model.

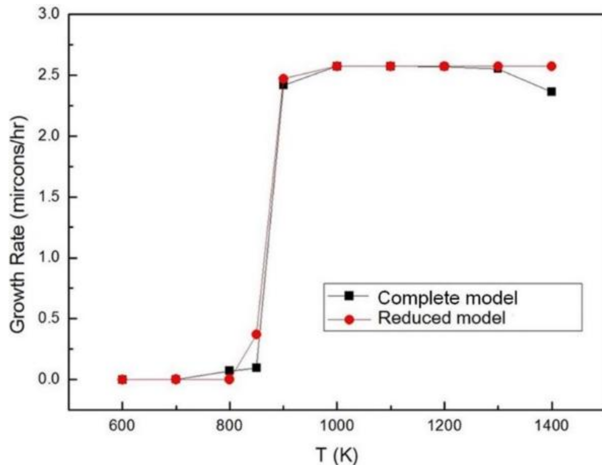

Fig. 10. Completemodel vs. the Reduced model.

C. *Mechanism optimization*

We investigated whether the mechanism (Reduced model) can be simplified further. As illustrated in Fig. 6, in a low-temperature zone, TMG tends to form an adduct with NH_3. However, in a high-temperature zone, all the TMG is rapidly consumed by DMG. Moreover, as displayed in Fig. 7, similar to TMG, in a high-temperature zone, all the DMG is consumed by MMG; however, DMG tends to form an adduct with NH_3 in a low-temperature area. However, as illustrated in Fig 8, at a high temperature, MMG participates in the ring reaction at the wafer surface; therefore, for a blue-LED process, we can perform the next simplified procedure.

In a high-temperature zone, we assume that all TMG is consumed to immediately form MMG, and the adduct assumption is negligible. Therefore, for a gas reaction, the mechanism can be reduced to only one chemical reaction, and the reaction for adduct is negligible; Table 6 presents the results (New model).

Table 6
New mechanisms (New model) for GaN deposition.

	Gas Reaction, $k=AT^n e^{-Ea/RT}$	A	n	Ea
1	TMG → MMG + C_2H_6	1.00E+47	1.00E+47	-9.18
	Surface Reaction			
2	TMG + N(S) → TMG(S)	1.16E+05	2.98	0
3	TMG(S) → TMG + N(S)	1.12E+14	0.55	49675
4	NH_3 + TMG(S) → TCOM1(S)	3.35E+07	3.33	0
5	TCOM1(S) → NH_3 + TMG(S)	5.70E+13	-0.161	11922
6	TCOM1(S) → $3CH_4$ + GaN(B) + N(S)	1.49E+11	0.609	49675
7	MMG + N(S) → MMG(S)	1.16E+05	2.98	0
8	MMG(S) → MMG + N(S)	1.12E+14	0.55	107673
9	NH_3 + MMG(S) → COMPM1(S)	3.35E+07	3.33	0
10	COMPM1(S) → NH_3 + MMG(S)	5.70E+13	-0.16	8146
11	COMPM1(S) → H_2 + GaN(B) + N(S) + CH_4	3.68E+09	2.05	59610

Fig. 11 provides the final predicted results of the Complete model, Reduced model, and New model, and the experimental data of their comparisons. The difference between the New model and the Complete model is low.

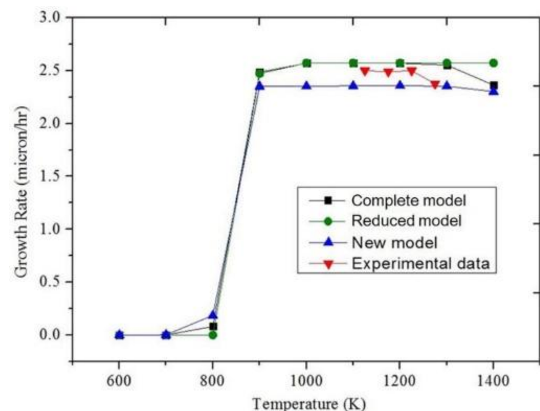

Fig. 11. Comparison among all mechanism models.

The pressure effect of growth rate for New model

Fig. 12 provides the pressure effect of GaN thin film growth rate for New model in different temperature, the pressure effect is significant only on 1400K. When the low temperature reaction, the GaN reaction mechanism is dominant by surface kinetic, so the pressure is not a key factor in low temperature. In 1400K, the growth rate is change when the reaction pressure lower than 200torr, this is contributed by the reduced for residence time.

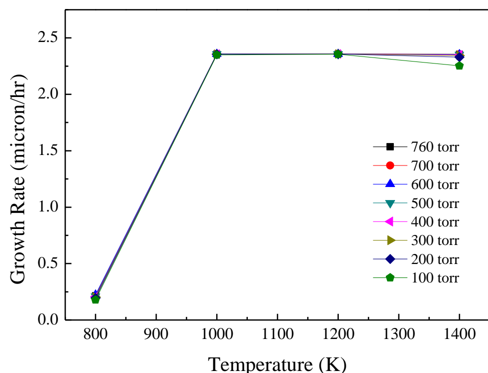

Fig. 12. The pressure effect for the New model

The III/V ratio effect of growth rate for New model

Fig. 13, 14 provides the effect of NH_3 and TMGa, we can clearly see that the TMGa is the dominant species in the full New mechanism model, when the gas flow rate of the NH_3 increase, the residence time is reduced, but this effect is lower than surface reaction by NH_3.

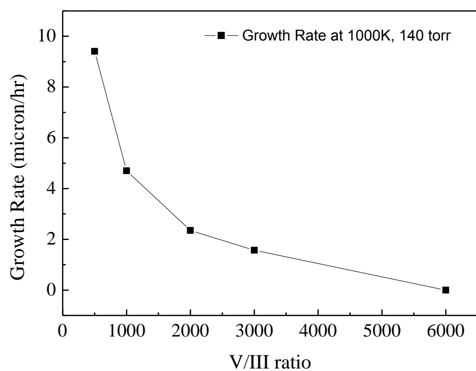

Fig. 13. The effect of V/III ratio (The flow rate of species V is constant)

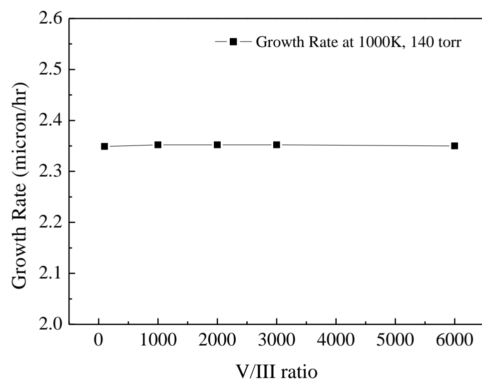

Fig. 14. The effect of V/III ratio (The flow rate of species III is constant)

D.Numerical analysis of the 2D model

In this section, we consider the new model mechanism as an input parameter for 2D calculation. Table 7 lists the input parameters and numerous boundary conditions for 2D computation, and Figs. 15(a) and (b) illustrate the reactor shapes for Experiments 1 and 2, respectively.

Table 7

Process parameters for 2D computation.

Volume flow rate		
Standard condition		
	2-D Experiment 1	2-D Experiment 2
TMGa flow rate (Slm) NH_3 flow rate (Slm) H_2 flow rate (Slm)	7.48×10^{-4} 2 10	3×10^{-3} 6 7.1
Real condition		
	2-D Experiment 1	2-D Experiment 2
TMGa flow rate (lm) NH_3 flow rate (lm) H_2 floe rate (lm)	6.24 × 10-3 16.7 83.5	1.8×10^{-2} 36 42
Parameter		
Initial pressure (torr)	100	140
Susceptor temperature (K)	1323	1323
Wall temperature (K)	300	300
Operating density (kg/m^3)	0.0241	0.0665
Reactor initial temperature (K)	300	300
Average molecular weight (amu)	4.5	8.893

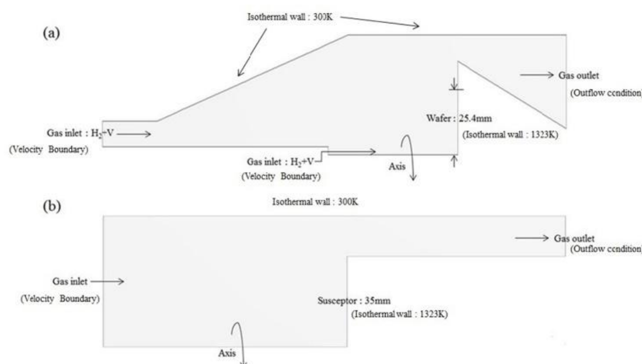

Fig. 15. Schematic diagram of (a) Experiment 1 [10] and (b) Experiment 2 [11].

Fig. 16 is the schematic diagram of meshfor each reactor. The first simulation experiment is performed for a simple vertical double-nozzle reactor, displayed in Fig. 15(a), for which the experimental data are provided by Table 7. The average growth rate is received at 1323 K.

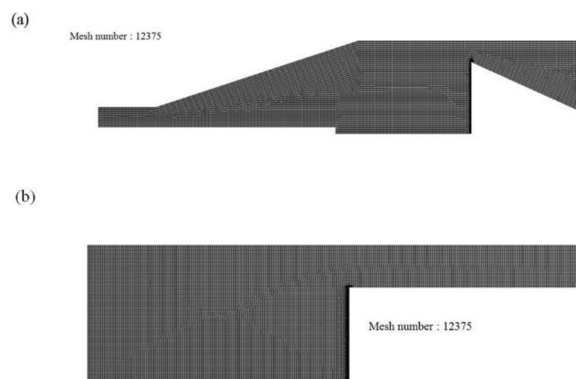

Fig. 16. Schematic diagram of mesh for (a) Experiment 1 [10] and (b) Experiment 2 [11].

Fig. 17 provides the results; the predicted growth rates agree well with the experimental data. For Reactor 1, the species of Group III appear from the inner nozzle, and those for Group V appear from the exterior nozzle. This reactor configuration implies that the growth rate of the inner wafer is extremely high and decreases from the wafer center to the outer edges. This is due to the species depletion as the reactant flow over the susceptor.

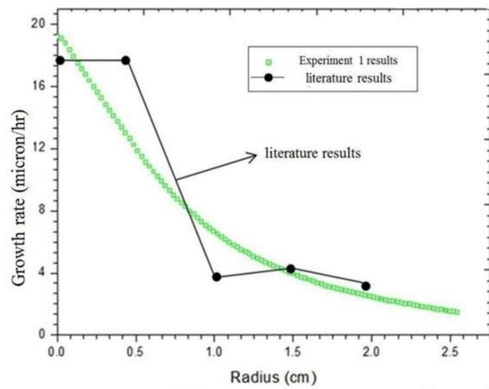

Fig. 17. 2D Experiment 1 result vs. literature results [10].

The second simulation set is performed for a vertical showerhead reactor, displayed in Fig. 15(b), for which the experimental data and boundary conditions are provided by Table 7. The average growth rate is received in the temperature range 1100–1300 K. The predicted growth rates agree well with the experimental data at each temperature point (Fig. 18).

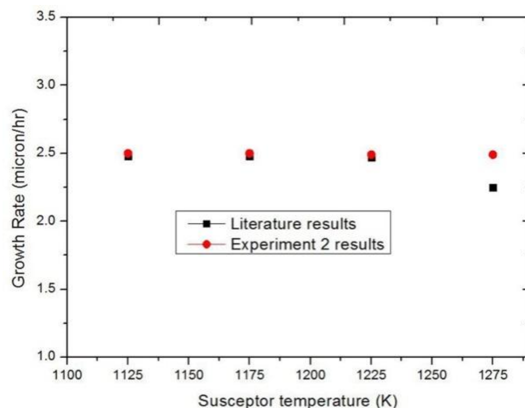

Fig. 18. 2D Experiment 2 results vs. literature results [11].

IV. Conclusions

A simplified process that used CHEMKIN for modeling the GaN growth is demonstrated. Several reaction pathways are calculated using ROP analysis. The activation barriers and vibrational frequencies are employed for calculating rate constants. The New mechanism (New model) is used for calculating the growth rate for different reactors through CFD. The average growth rate is achieved in the temperature range 1100–1300 K. The predicted growth rates agreed well with the experimental data at each temperature point. The most simplified mechanism can be used to predict the growth rate of a blue-LED process before an actual process begins; this is extremely useful for LED companies. All of these observations demonstrate that the proposed mechanisms are fairly universal and crucial pathways for the epitaxial growth of GaN.This study provides a useful and a predictable mechanism for GaN thin film research in blue-LED process.More verification work is under way by our own experiments.

V. Acknowledgments

This study was supported by the Department of Mechanical Engineering, National Central University, Taiwan (R.O.C)and Chung Yuan Christian University (R.O.C).Industrial Technology Research Institute, Taiwan (R.O.C).

REFERENCES

[1] G.B. Stringfellow,*Organometallic Vapor-Phase Epitaxy: Theory and Practice*, Salt Lake City, 1999. pp. 1-16.

[2] Y. Seki, K. Tanno, K. Lida and E. Ichiki, (1975, August). Properties of epitaxial GaAslayers from a tri-ethyl gallium and arsine system. *J. Solid State Sci. Technol.*[Online]. 122(8). pp. 1108-1112. Available: http://jes.ecsdl.org/content/122/8/1108.full.pdf

[3] R. R. Saxena, V. Aebi and C. B. Cooper, M. J. Ludowise, H. A. Vander Plas, B. R. Cairns, T. J. Maloney, P. G. Borden and P. E. Gregory. (1980, July). High-efficiency AlGaAs/GaAs concentrator solar cells by organometallic vapor phase epitaxy. *J. Appl. Phys.* [Online]. 51.pp. 4501-4503.Available:http://scitation.aip.org/content/aip/journal/jap/51/810.1063/1.328389

[4] H. Amano, M. Kito, K. Hiramatsu and I. Akasaki. (1989, November). P-type conduction in Mg-doped GaN treated with low-energy electron beam irradiation. *J. Appl. Phys.*[Online]. 28.pp. L2112-L2114. Available:http://iopscience.iop.org/article/10.1143/JJAP.28.L2112/meta

[5] S. Nakamura. (1991, October). GaN Growth Using GaN Buffer Layer.*J. Appl. Phys.* [Online]. 30.pp. L1705-1707. Available: http://iopscience.iop.org/article/10.1143/JJAP.30.L1705/meta

[6] S. Nakamura, T. Mukai, M. Senoh and N. Iwasa.(1992, February). Thermal Annealing Effects on P-Type Mg-Doped GaN Films. *J. Appl. Phys.* [Online]. 31.pp. L139-L142. Available:http://iopscience.iop.org/article/10.1143/JJAP.31.L139/meta

[7] S. Nakamura, T. Mukai and M. Senoh. (1993, January). Candela-class high-brightness InGaN/AlGaN double-heterostructureblue-light-emitting.*J. Appl. Phys.*[Online]. 64.pp. 1687-1689.Available:http://coen.boisestate.edu/bknowlton/files/2011/09/APL-Nakamura-Candela-class-high-brightness-InGaN-AlGaN-double-heterostructure-blue-light-emitting-diodes-19941.pdf

[8] C. K. Hu, H. I Chien, and Tomi T. Li. (2015, July). Numerical analysis for the growth of epitaxy layer in a large-size MOCVD reactor.*Key Eng. Mater.* [Online]. 656-657.pp. 515-519. Available:http://www.scientific.net/KEM.656-657.515

[9] C. K. Hu, Tomi T. Li, and Y. Lin. (2013, March). The optimization of thermal flow field in a large-size MOCVD reactor. *ECS Trans.* [Online]. 52(1).pp. 1021-1026. Available:http://ecst.ecsdl.org/content/52/1/1021.abstract

[10] S. A. Safvi, J. M. Redwing, M. A. Tischler and T. F. Kuech. (1997, May). GaN Growth by Metallorganic Vapor Phase Epitaxy. *J. Electrochem. Soc.*[Online]. 144(50). pp. 1789-1796 Available:http://jes.ecsdl.org/content/144/5/1789.short

[11] C. Theodoropoulos, T. J. Mountziaris, H.K. Moffat and J. Han. (2000, July). Design of gas inlets for the growth of gallium nitride by metalorganic vapor phase epitaxy. *J. Cryst.* [Online].*Growth*. 217. pp. 65-81. Available:http://www.sciencedirect.com/science/article/pii/S0022024800004024

[12] J. Sun, J. M. Redwing and T. F. Kuech, (1999, November). Transport and Reaction Behaviors of Precursors during Metalorganic Vapor Phase Epitaxy of Gallium Nitride. *Phys. Status Solidi A*. [Online]. 176. pp.693-698. Available:http://onlinelibrary.wiley.com/doi/10.1002/(SICI)1521-396X(199911)176:1%3C693::AID-PSSA693%3E3.0.CO;2-Z/abstract

[13] A. Hirako, K. Kusakabe, and K. Ohkawa, (2005, February). Modeling of Reaction Pathways of GaN Growth by Metalorganic Vapor-Phase Epitaxy Using TMGa/NH3/H2: System: A Computational Fluid Dynamics Simulation Study. *J. Appl. Phys.* [Online]. 44(2). pp. 874-879. Available:http://iopscience.iop.org/article/10.1143/JJAP.44.874/meta

[14] R. P. Parikh and R. A. Adomaitis.(2006, September). An overview of gallium nitride growth chemistry and its effect on reactor design: Application to a planetary radial-flow CVD system. *J. Cryst. Growth*,[Online]. 286.pp. 259-278.
Available:https://www.researchgate.net/publication/222567111_An_overview_of_gallium_nitride_growth_chemistry_and_its_effect_on_reactor_design_Application_to_a_planetary_radial-flow_CVD_system

[15] D. Sengupta, S. Mazumderb, W. Kuykendall and S. A. Lowry.(2005, March). Combined ab initio quantum chemistry and computational fluid dynamics calculations for prediction of gallium nitride growth. *J. Cryst. Growth*, [Online]. 279.pp. 369-382.
Available:http://www.sciencedirect.com/science/article/pii/S0022024805002149

[16] G. H. Evans and R. Greif. (2009, October). A Numerical Model of the Flow and Heat Transfer in a Rotating Disk Chemical Vapor Deposition Reactor. *J. Heat Transfer*, [Online]. 109(4).pp. 928-935.
Available:http://heattransfer.asmedigitalcollection.asme.org/article.aspx?articleid=1439491

[17] R.Zuo, H. Zhang and X. L. Liu.(2006, August). Transport phenomena in radial flow MOCVD reactor with three concentric vertical inlets. *J. Cryst. Growth*, [Online]. 293(2).pp. 498-508.
Available:http://www.sciencedirect.com/science/article/pii/S002202480600546X

[18] C. Y. Soong, C. H.Chyuan and R. Y.Tzong, (1998, October). Thermo-Flow Structure and Epitaxial Uniformity in Large-Scale Metalorganic Chemical Vapor Deposition Reactors with Rotating Susceptor and Inlet Flow Control. *J. Appl. Phys.*[Online]. 37. pp-5823 5839.
Available:http://iopscience.iop.org/article/10.1143/JJAP.37.5823/meta

[19] D. I. Fotiadis, S. Kieda and J. F. Jensen, (1990, September). Transport phenomena in vertical reactors for metalorganic vapor phase epitaxy: I. Effects of heat transfer characteristics, reactor geometry and operating conditions. *J. Cryst. Growth,*102, 441-470.
Available:http://www.sciencedirect.com/science/article/pii/0022024890904038